Polymer 51 (2010) 2818–2824

Contents lists available at ScienceDirect

Polymer

journal homepage: www.elsevier.com/locate/polymer

Reversible thermoflocculation of magnetic core–shell particles induced by remote magnetic heating

Thorsten Gelbrich [1], Gernot U. Marten, Annette M. Schmidt*

Institut für Organische Chemie und Makromolekulare Chemie, Heinrich-Heine-Universität Düsseldorf, Universitätsstr. 1, D-40225 Düsseldorf, Germany

ARTICLE INFO

Article history:
Received 13 September 2009
Received in revised form
31 January 2010
Accepted 19 February 2010
Available online 1 March 2010

Keywords:
Thermoresponsive magnetic nanoparticles
LCST
Magnetic heating

ABSTRACT

We developed multifunctional magnetic polymer brushes with a tailorable thermoresponsive dispersion behavior that can be activated by AC magnetic fields. Via surface-initiated ATRP, magnetic core–shell nanoparticles are obtained that are composed of nanosized superparamagnetic iron oxide cores and a copolymer shell. The shell consists of oligo(ethylene glycol) methylether methacrylate (OEGMA) and methoxyethyl methacrylate (MEMA) copolymers that show a lower critical solution temperature (LCST) in water.

The hybrid structures are easily dispersible in water at room temperature, and show a reversible thermoflocculation at critical temperatures adjustable by the copolymer composition. The phase separation can alternatively be initiated and recorded by magnetic heating caused by magnetic losses in AC fields. This method offers a convenient way for the remote-controlled heating and agglomeration of disperse systems.

1. Introduction

The possibility to control material properties by external stimuli is of considerable importance for the development of novel technologies for actuation, sensing, and pumping, e.g. in microfluidic devices. Recently, thermosensitive polymers have been combined with nanoparticles in order to achieve a reversible phase transition in water and other media. [1,2,3,4,5,6,7,8]. The polymers show a thermoreversible change in solubility, referred to as a lower or upper critical solution temperature (LCST/UCST) behavior.

By combining thermoresponsive polymers with magnetic nanoparticles, hybrid materials become possible that can be manipulated by two different stimuli; temperature and magnetic fields. Such dual responsive materials are of interest for a variety of applications ranging from magnetic separation or drug release systems to sensors and actuation [8,9].

We, and other groups, have demonstrated, that magnetite nanoparticles decorated with a stabilizing shell composed of LCST or UCST polymers lead to nanocomposites that show thermally inducible flocculation behavior in the carrier medium [3,6,10,11,12,13,14,15]. The single particles agglomerate at a critical temperature resulting in an enhanced magnetic response. Thus the particle agglomerates can be separated easily by low magnetic field gradients, and facilitate, for instance, the separation process in purification applications of biomolecules.

For water-based thermoresponsive magnetic hybrid systems most often poly(N-isopropylacrylamide) (PNiPAAm) is chosen as the polymeric stabilizing shell because of its LCST (32 °C) which is near to body temperature and nearly insensitive to environmental conditions such as ionic strength and pH [16,17]. Magnetite (Fe_3O_4) or maghemite (γ-Fe_2O_3) are predominantly used as magnetic nanoparticles due to their biocompatibility, well understood properties, and easy synthesis. Recently, Chanana et. al. have presented nanocomposites based on magnetite and thermoresponsive poly(oligo(ethylene glycol) methacrylate) (POEGMA) copolymers [18]. The advantage of these polymers compared to PNiPAAm is that the LCST in water is easily adjustable by the oligo(ethylene glycol) chain length in a wide temperature range. Furthermore PEG derivatives are known to be biocompatible and to avoid protein adsorption on surfaces [19,20].

The magnetic interaction of the nanoparticles is not limited to the attractive forces that are used in separation applications. Magnetic nanoparticles can also be used as heat generators. In AC magnetic fields in the kHz range, the nanoparticles transform magnetic energy to heat energy due to relaxation processes and hysteresis losses [21,22,23]. This remote-controlled way of heat generation is under intensive investigation for cancer therapy in *magnetic fluid hyperthermia* [24,25].

* Corresponding author. Tel.: +49 211 8114820; fax: +49 211 15840.
E-mail address: schmidt.annette@uni-duesseldorf.de (A.M. Schmidt).
[1] Current address: Qiagen GmbH, Hilden, Germany.

0032-3861/$ – see front matter © 2010 Elsevier Ltd. All rights reserved.
doi:10.1016/j.polymer.2010.02.032

In the present report, we discuss the preparation and characterization of magnetic core–shell nanoparticles that show a fully reversible and tailorable thermoflocculation in water. The thermosensitive brush-like polymer shell is obtained via surface-initiated ATRP of methacrylates with hydrophilic side chains. The resulting magnetic polymer brush particles are superparamagnetic, show a high grafting density, and exhibit a thermoresponsive dispersion behavior in water due to a LCST of the polymer arms. By exposure of the obtained nanoparticle dispersions to an AC magnetic field, we are able to heat the fluids by remote control to temperatures above LCST so that the phase transition occurs. From the obtained heating behavior we collect calorimetric data that are compared to conventional DSC results.

2. Experimental section

2.1. Materials

2,2'-Bipyridine (bpy) (Aldrich, 99%), 2-bromo-2-methyl-propionic acid tert-butyl ester (Aldrich, 98%), copper(I) bromide (CuBr) (Aldrich, 98%), oligo(ethylene glycol) methylether methacrylate (OEGMA, Aldrich, $M_n = 290\ g\ mol^{-1}$) are used as received without further purification. 2-Methoxyethyl methacrylate (MEMA, Aldrich, 99%) is distilled under reduced pressure and stored under argon. Dimethylsulfoxide (DMSO) is dried by heating over calcium hydride (Riedel-de-Haen) for 2 h, followed by distillation under reduced pressure.

2.2. ATR copolymerization of OEGMA and MEMA in DMSO solution

Copper(I) bromide (36.5 mg, 0.26 mmol), 2,2'-bipyridine (100.0 mg, 0.64 mmol) and 2-bromo-2-methyl-propionic acid tert-butyl ester (48 μl, 0.26 mmol) were added to a Schlenk flask. Afterwards, the flask was degassed and subsequently purged with argon three times. Then 5.0 ml degassed DMSO was added for dissolution. The polymerization was started by addition of a degassed mixture of MEMA and OEGMA (20 mmol total monomer content). The reaction was carried out for 72 h at ambient temperature. The polymer fraction was isolated by precipitation with ether/acetone.

2.3. Polymer brush-decorated magnetic particles

The synthesis of the employed FeO_x nanoparticles (with a composition close to Fe_3O_4) and the surface immobilization of 2-bromo-2-methylpropionic acid (BMPA), is described in detail elsewhere [11,12]. The surface-initiated ATRP of MEMA and OEGMA is performed by dissolving 43.0 mg (0.30 mmol) CuBr and 120 mg (0.77 mmol) bpy in 12 ml of a DMSO based FeO_x@BMPA particle dispersion ($c(FeO_x) = 0.83\ mg\ ml^{-1}$), and heating to 50 °C. To start the polymerization, the respective mixture of the two comonomers MEMA and OEGMA (10 mmol of total monomer) is added. The comonomer ratio is varied to achieve copolymer shells with a MEMA content between 0 and 50 mol-%. The reaction is carried out for 5 d stirring at room temperature. Afterwards, the obtained core–shell nanoparticles are transferred to aqueous carrier media by particle precipitation from DMSO dispersions using diethyl ether, magnetic separation, washing and redispersion in water.

2.4. Core acidolysis of magnetic brush particles

In order to isolate and characterize the polymer arms of the obtained core–shell structures, 1 ml of the obtained DMSO-based FeO_x@P(OEGMA-*co*-MEMA) particle dispersion is precipitated by adding diethyl ether. After magnetic separation and several washing steps with diethyl ether, the particle precipitate is redispersed in 2 ml of 3 M hydrochloric acid. The FeO_x cores of the hybrid materials were dissolved under the influence of the acid, resulting in a yellow solution. For the separation of the copolymers, the mixture is heated, resulting in a precipitation of the copolymers above the LCST. The supernatant is decanted, and fresh water is added to the polymer precipitate. This procedure is repeated until the supernatant is practically colorless. The copolymers are analyzed by GPC and NMR.

2.5. Analytic methods and instrumentation

ATR-IR spectra are measured on a Nicolet 6700 spectrometer. Elemental analysis is performed on a Perkin–Elmer 2400 CHN analyzer. For TGA, a Netzsch STA 449c in a He atmosphere is used with a heating rate of $10\ K\ min^{-1}$ between 30 and 600 °C. Gel permeation chromatography (GPC) elugrams are collected on THF ($300 \times 8\ mm^2$ MZ Gel Sdplus columns, Waters 410 RI-detector) relative to polystyrene standards. NMR spectroscopy is performed on a Bruker DRX500 at 500 MHz and ambient temperature. DLS experiments are performed on a Malvern HPPS-ET. The particle size distribution is derived from a deconvolution of the measured intensity autocorrelation function of the sample by the General Purpose Mode (non-negative least-squares) algorithm included in the DTS software. Each experiment is performed at least three times. Turbidity curves are collected on a Tepper TP1 cloud point photometer. From the turning point of the turbidity curves the cloud point temperature T_c is obtained. Vibrating sample magnetization (VSM) measurements are implemented on a ADE Magnetics

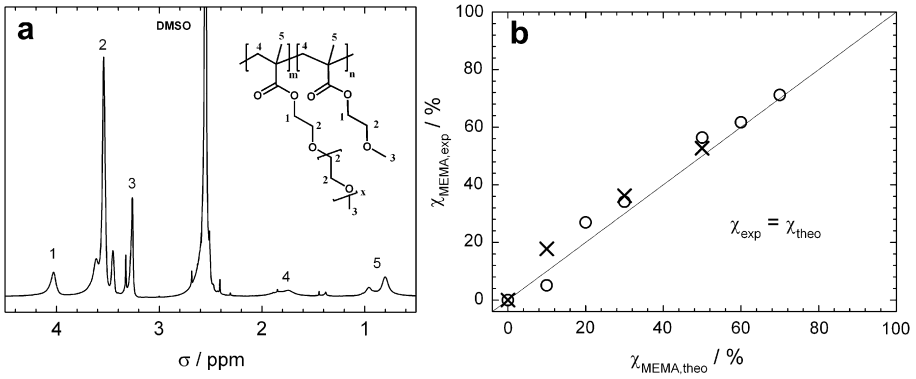

Fig. 1. (a) ^{1}H-NMR spectrum of model copolymer P(OEGMA-co-MEMA)27; (b) experimentally determined molar fraction of MEMA $\chi_{MEMA,exp.in}$ of model poly(OEGMA-*co*-MEMA) copolymers (crosses), and in polymer brush particle shells (circles), vs. initial MEMA fraction $\chi_{MEMA,theo}$ in the comonomer mixture.

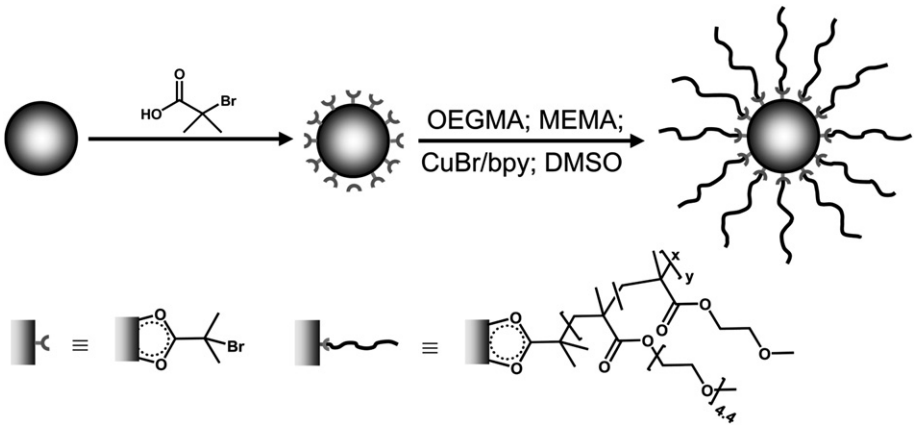

Scheme 1. Synthesis of FeO_x@P(OEGMA-*co*-MEMA) magnetic polymer brush particles by surface-initiated ATRP.

vibrating sample magnetometer EV7. Induction heating experiments are performed on a Hüttinger HF generator Axio 5/450 T equipped with a copper inductor ($l = 50$ mm, d$I = 35$ mm, $n = 5$), and operating at 250 kHz and a magnetic field of 31.5 kA m^{-1}. Differential Scanning calorimetry thermograms are collected on a Mettler-Toledo DSC 822^e at 5 K min^{-1}.

3. Results and discussion

Based on our recent work on the synthesis of magnetic brush particles, and more recent works by others [11,18,20,26,27] we here report the synthesis of water-dispersible nanostructures composed of a magnetic core and P(OEGMA-*co*-MEMA) brush shell. The thermoflocculation behavior of the particles in water is investigated by different methods using conventional and magnetic heating.

The polymerization behavior of the two comonomers of choice, MEMA and OEGMA (see Fig. 1), and the dependence of the critical solution temperature on the composition are analyzed on model copolymers.

Thermoresponsive magnetic polymer brushes are formed by surface-initiated copolymerization of MEMA and OEGMA in DMSO by using FeO_x@BMPA nanoparticles as macroinitiators (see Scheme 1).

3.1. Model copolymers

In order to investigate the polymerization characteristics of the comonomer system of choice under ATRP conditions, and to validate the reaction conditions as well as the properties of the resulting copolymers, we present results on a series of model copolymers prepared from OEGMA and MEMA in DMSO at 50 °C with CuBr/bpy (1:2) as the catalyst. As initiator, we employed 2-bromo-2-methyl-propionic acid tert.-butyl ester as a low molecular analogue for the functionalized particles. While the total monomer-to-initiator ratio was chosen to result in a apparent molar mass of 20,000 g mol^{-1}, we varied the initial monomer composition between 0% and 70% of MEMA. The obtained copolymer composition, molecular weight, and molecular weight distribution are presented in Table 1 together with the thermal properties of their aqueous solutions.

A typical ^{1}H-NMR spectrum of the copolymers in D_2O is shown in Fig. 1a for P(OEGMA-*co*-MEMA)27. The signals of the spectrum can be assigned to the copolymer protons as indicated in the figure inset [28]. The copolymer composition is determined from the spectra using the intensity ratio of signals 1 and 2 as a measure of the average side chain length in the copolymer. From this value, we can easily calculate the molar ratio of the two comonomers and their distinct side chain length.

The obtained values for the molar fraction of MEMA $\chi_{MEMA,exp}$ in the copolymers correspond well with the MEMA molar fraction $\chi_{MEMA,theo}$ expected from the monomer feed (Fig. 1b). This is in agreement with the high conversion (>90% in all runs). In addition, the molar masses determined by GPC are close to the initial monomer-to-initiator ratio of 20,000 g mol^{-1}.

However, the molecular weight distribution, as indicated by polydispersity index M_w/M_n of up to 2, is higher than expected for an ideally controlled reaction. This observation is in agreement with reports of others, indicating that a comparably slow initiation process of the BMPM/CuBr/bpy system in methacrylate ATRP [28,29,30], combined with a relative high initial monomer concentration (4 mol l^{-1}). We achieved substantial advancement by using CuCl instead of CuBr, thus slowing down the propagation step, and amending the rate of initiation and propargation. However, in the course of the project, the CuCl system proved to be inefficient in the corresponding surface-initiated polymerization protocols. For the preparation of hybrid particles, we therefore stayed with the CuBr/bpy system.

All obtained copolymers with the exception of P(OEGMA-co-MEMA)71 are well-dispersible in water at room temperature. Yet, as previously shown for similar copolymers containing oligo (ethylene glycol) methacrylate monomers with different side chain lengths, they possess lower critical solution behavior in water [31,32,33] that can be adjusted by the copolymer ratio. Below the phase transition temperature, the formation of stabilizing hydrogen bonds between solvating water molecules and ether oxygen atoms of the hydrophilic side chains counteract the hydrophobic effect of the carbon backbone [34], and the polymers exhibit good water solubility. With increasing temperature,

Table 1
Molecular weight, composition, and cloud point temperatures of P(OEGMA-*co*-MEMA) model copolymers.[a]

Sample[a]	$\mu_{MEMA,exp}$ (%)	$M_{n,\ app}$ (g mol^{-1})	M_w/M_n	T_c (°C)
P(OEGMA-*co*-MEMA)71	71	19,390	1.96	22.8
P(OEGMA-*co*-MEMA)62	62	19,700	2.03	31.4
P(OEGMA-*co*-MEMA)57	57	22,860	2.07	36.9
P(OEGMA-*co*-MEMA)34	34	20,460	1.78	47.2
P(OEGMA-*co*-MEMA)27	27	18,350	1.71	53.2
P(OEGMA-*co*-MEMA)5	5	15,860	1.70	56.8
POEGMA	0	11,350	1.40	65.4
POEGMA[b]	0	13,950	1.13	n.d.

[a] Sample annotations: P(OEGMA-*co*-MEMA)[$\chi_{MEMA,exp}$]; $\chi_{MEMA,exp}$, molar fraction of MEMA in copolymers (by ^{1}H-NMR); $M_{n,\ app}$, apparent number average molar mass relative to PS (GPC); M_w/M_n, polydispersity index (by GPC); T_c, cloud point temperature (by CPP).
[b] Prepared by replacing CuBr with CuCl during synthesis.

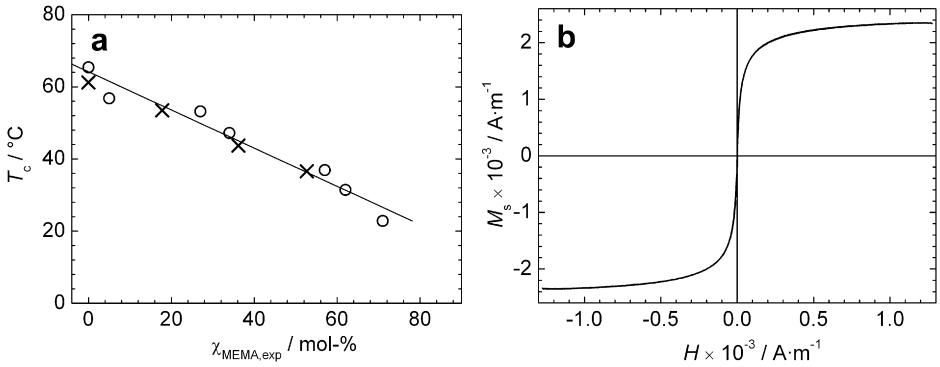

Fig. 2. (a) Cloud point temperature T_c of P(OEGMA-co-MEMA) model copolymers (circles) and of FeO_x@P(OEGMA-co-MEMA) (crosses) in water in relation to molar fraction of MEMA $\chi_{MEMA,exp}$ in the polymer fraction; (b) VSM loop of saturated magnetic fluid based on FeO_x@P(OEGMA-*co*-MEMA)36 nanoparticles in DMSO.

thermal fluctuations antagonize the hydrogen bond flocculation. At a relatively narrow temperature range depending on the shell composition, flocculation is observed, and allows the determination of the cloud point temperature T_c by cloud point photometry (CPP) [11,12].

In the series of the presented copolymers, we find an almost linear correlation of T_c with the composition (Fig. 2a). This can be attributed to the gradual change in the polymer-solvent interaction quality with respect to the composition and is mainly ascribed to the variation in density of the longer side chains along the molecule. We will show below that this behavior can be used to magnetically induce a thermoflocculation of core–shell particles caused by magnetic heating.

3.2. Core–shell particle synthesis and characterization

For the preparation of hybrid particles, we employed polymerization conditions comparable to model copolymer synthesis in the presence of initiator-functional magnetic particles. We obtained core–shell objects with polymer shells of different copolymer compositions that are easily dispersible in DMSO, DMF, $CHCl_3$, and water.

In the first step, FeO_x nanoparticles are prepared by alkaline precipitation based on a method of Cabuil and Massart [35] and is described, as well as the surface functionalization of FeO_x nanoparticles with 2-bromo-2-methylpropionic acid (BMPA), in detail elsewhere [11,12].

The surface-initiated copolymerization of OEGMA and MEMA was performed with BMPA functionalized magnetite nanoparticles as macroinitiators suspended in DMSO at 50 °C in the presence of CuBr/bpy. From the obtained black particle dispersions, the core–shell particles were isolated and purified by repeated precipitation, washing, and magnetic separation cycles before redispersion in water. The particles are easily redispersed in water up to 5 mass-% of solid. The obtained particle dispersions are stable against agglomeration fields for several months at neutral pH, as has been shown by DLS experiments. However, at a reduced pH of 5, aging of the samples is observed by precipitation of the magnetic cores and detectable amounts of free polymer chains in the supernatant indicating the hydrolysis of the acid based surface anchor.

In order to confirm the success of the polymerization, ATR-IR spectra of carefully washed and dried particles were taken. Fig. 3a compares the spectrum of FeO_x@POEGMA to those of BMPA functionalized and bare FeO_x nanoparticles.

We observe intensive peaks that are assigned to the presence of POEGMA or its copolymers with MEMA in the spectra of all polymer-modified particles, including signals assigned to the methyl and methylene groups (2875 cm^{-1}, b), the C=O double bond (1714 cm^{-1}, s), the C–O single bonds (1101 cm^{-1}, b) and several peaks in the fingerprint region at 1356, 1251, 1196, 1060 and 1022 cm^{-1} that are also found in the ATR-IR spectrum of the free polymer. The ATR-IR spectra of FeO_x@P(OEGMA-*co*-MEMA) particles with different shell composition show no qualitative difference.

The composition of the obtained hybrid materials is analyzed by thermogravimetric measurements. In Fig. 3b the sample mass loss of dry FeO_x@P(OEGMA-*co*-MEMA) nanoparticles in TGA is shown over the sample temperature *T*. A mass loss of 33–63% is observed between 200 °C and 480 °C that can be attributed to the decomposition of the polymeric shell, with a maximum degradation rate at 300 °C. A two-stage decomposition is observed for the particles

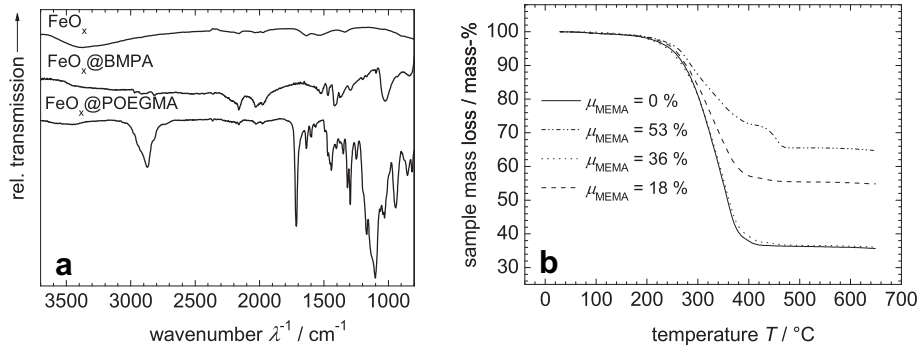

Fig. 3. (a) ATR-IR spectra of as synthesized FeO_x nanoparticles, BMPA functionalized FeO_x particles and FeO_x@OEGMA magnetic polymer brushes; (b) sample mass loss vs. sample temperature *T* in TGA experiments on FeO_x@P(OEGMA-*co*-MEMA).

Table 2
Composition of investigated FeO_x@P(OEGMA-*co*-MEMA) core–shell nanoparticles.[a]

Sample[a]	$\chi_{MEMA,theor}$ (mol-%)	$\chi_{MEMA,exp}$ (mol-%)	$M_{n,app}$ (g/mol)	M_w/M_n	μ_P (wt.-%)	$d_{h,n}$ (nm)	d_c (nm)	μFeO_x (wt-%)	T_c^h (°C)
FeO_x@POEGMA	0	0	67100	1.2	62.9	169	10.2	2.10	61.2
FeO_x@P(OEGMA-*co*-MEMA) 18	10	17.8	35900	1.4	43.8	127	10.7	1.91	53.4
FeO_x@P(OEGMA-*co*-MEMA) 36	30	36.2	65270	1.8	62.8	171	10.5	2.48	43.7
FeO_x@P(OEGMA-*co*-MEMA) 53	50	52.7	36100	1.3	33.8	113	10.3	1.22	36.6

[a] FeO_x@P(OEGMA-*co*-MEMA)[$\chi_{MEMA,exp}$], μ_P, mass fraction of copolymer in dry particle powder (TGA); μFeO_x, mass content of FeO_x in saturated DMSO dispersion (VSM); $d_{h,n}$, number average hydrodynamic diameter (DLS); d_c, volume average core diameter (VSM); M_n, apparent number average molar mass relative to PS (GPC); M_n/M_W, polydispersity index (GPC); $\chi_{MEMA,theor}$, theoretical MEMA mol content from comonomer ratio; $\chi_{MEMA,exp}$, obtained MEMA content in copolymers (^{1}H-NMR); T_c, cloud point temperature (CPP).

with the highest MEMA content. The lower polymer fraction obtained for FeO_x@P(OEGMA-co-MEMA)18 and FeO_x@P(OEGMA-co-MEMA)53 can be explained by incomplete conversion during synthesis.

The polymer chain density can be determined to 0.26 mmol g^{-1} or 500 polymer chains per particle by using the number average molecular weight of the polymer arms as obtained by GPC. This value indicates a high initiator efficiency, taking into account the initiator density on the particle surface of 0.26 mmol g^{-1} as obtained by TGA, and 0.33 mmol g^{-1} obtained by elemental analysis. The values can be compared to the grafting density of similar materials obtained by a "grafting trough" method reported by Wang et al. of 150–200 chains per particle. [18].

The composition of the polymer shell and the molecular weight of the brush arms become accessible after acidolysis of the core for a part of the sample and isolation of the polymer fraction. The mild conditions of acidolysis have been proven to be harmless to the polymer, as confirmed by control experiments. The isolated polymers are characterized in solution using ^{1}H-NMR and GPC.

The results can be found in Table 2. The molecular weights are in the range of 30–70,000 g mol^{-1}, with low polydispersity indices (PDI) between 1.2 and 1.4 (and one exception). The PDI values are lower compared to those obtained for the model copolymers (see Table 1). We dedicated this to the lower initial monomer concentration (0.8 mol l^{-1}) in case of the surface-initiated ATRP that may lead to a better control of the reactions.

As for the composition, we find in all cases an acceptable agreement to the initial comonomer mixture during synthesis. By dynamic light scattering, hydrodynamic diameters between 113 nm and 169 nm are found, which are in agreement with the sizes of single-cored brush particles expected for their respective molecular weight by using a blob model for curved surfaces [36].

By quasi-static magnetization experiments, we obtain information on the magnetic properties of the particle dispersions (see Fig. 2b). A sigmoidal field-dependent magnetization curve is obtained, with a negligable coercitivity indicating a superparamagnetic behavior. From the saturation magnetization M_S for $H \rightarrow \infty$, the FeO_x mass content is accessible, indicating mass fractions of the magnetic cores between 1.2 mass-% and 2.5 mass.% (see Table 2). From the initial coercitivity $\chi_{ini} = (M/H)_{H\rightarrow 0}$, we calculate the volume average core diameter d_c according to Chantrell's method, resulting in values between 10.2 nm and 10.7 nm for all samples [37]. This observation indicates an individual response of the single nanoparticles to the magnetic field.

3.3. Thermoflocculation

The polymer brushes on the particle surface serve as dispersion stabilizers when brought to a medium that is a good solvent for the shell. Thus, in aqueous media, the hybrid particles show thermoresponsive behavior [18]: while readily dispersible at low temperature, they reversibly flocculate when the dispersion temperature reaches the T_c of the shell. Phase separation is the consequence.

In Scheme 2, the effect is shown schematically and in photographs of a water-based particle dispersion. Below T_c, the stabilizing effect of the solvated shell is active, and the particles form stable dispersions up to 5% solid. With strong magnets, the fluid can be manipulated as a whole against gravity, and the particles are not separated from the fluid. In contrast, above the T_c, the shell collapses and leads to particle agglomeration. As a consequence, the particles can be easily separated with a magnet. The phase transition is fully reversible so that a stable magnetic fluid is reformed after cooling below the LCST of the copolymeric shell.

We determine the cloud point temperatures T_c of the hybrid particles with different shell composition by CPP, and compare the results to the hydrodynamic diameter d_h in water obtained by DLS (see Fig. 4).

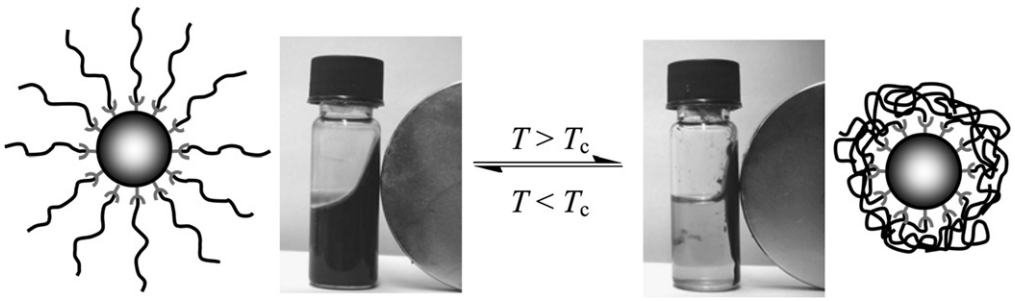

Scheme 2. Thermoflocculation of magnetic core–shell particles (here: FeO_x@P(OEGMA-co-MEMA)36) in water.

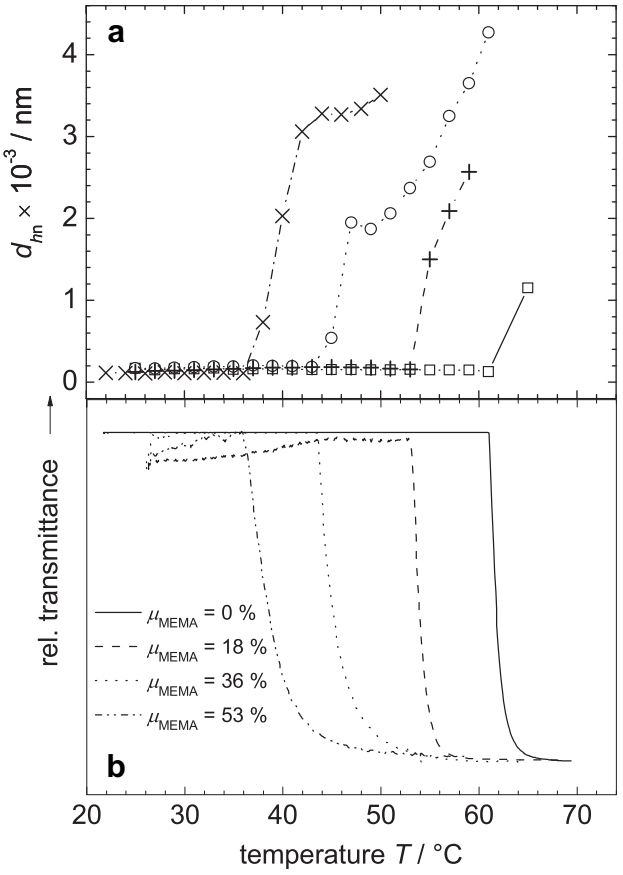

Fig. 4. (a) Number average hydrodynamic diameter d_{hn} (DLS) vs temperature T; (b) relative transmittance vs temperature T (CPP): compact line: FeO_x@P(OEGMA); dashed line: FeO_x@P(OEGMA-*co*-MEMA)18; dotted line: FeO_x@P(OEGMA-*co*-MEMA)36; dashed dotted line, FeO_x@P(OEGMA-*co*-MEMA)53.

Both methods indicate well-dispersed nanoparticles for all batches at 25 °C. Similar to the model polymers, particle dispersions show a sudden decrease of the transmittance upon heating, while in DLS, we observe a dramatic increase of the hydrodynamic diameter in the same temperature range. Both observations are caused by the agglomeration of the core–shell particles at T_c, and the two methods are in good agreement for all investigated samples.

We extract T_c from the turning points of the CPP graphs, and find a dependence of T_c on the shell composition that is in full accordance to the results of the model polymers (see Fig. 2). A linear relationship between T_c and $\chi_{MEMA,exp}$ is confirmed, that allows the easy tailoring of the thermoflocculation temperature of core–shell particles by the shell composition.

3.4. Behavior in AC magnetic fields

The ability of superparamagnetic nanoparticles to locally develop heat when exposed to external AC magnetic fields in the kHz range is of considerable interest to activate physical or chemical processes in the vicinity of the particles, e.g. in hyperthermia [24,25], and for the remote operation of thermoresponsive soft actuators [38]. The heat development occurs due to relaxational processes (Neél and Brown) as well as hysteresis effects that results in considerable losses during the dynamic magnetic response of the materials [21,39,40].

We investigated the behavior of FeO_x@P(OEGMA) dispersions in an oscillating magnetic field (250 kHz, $H = 31.5$ kA m^{-1}). The

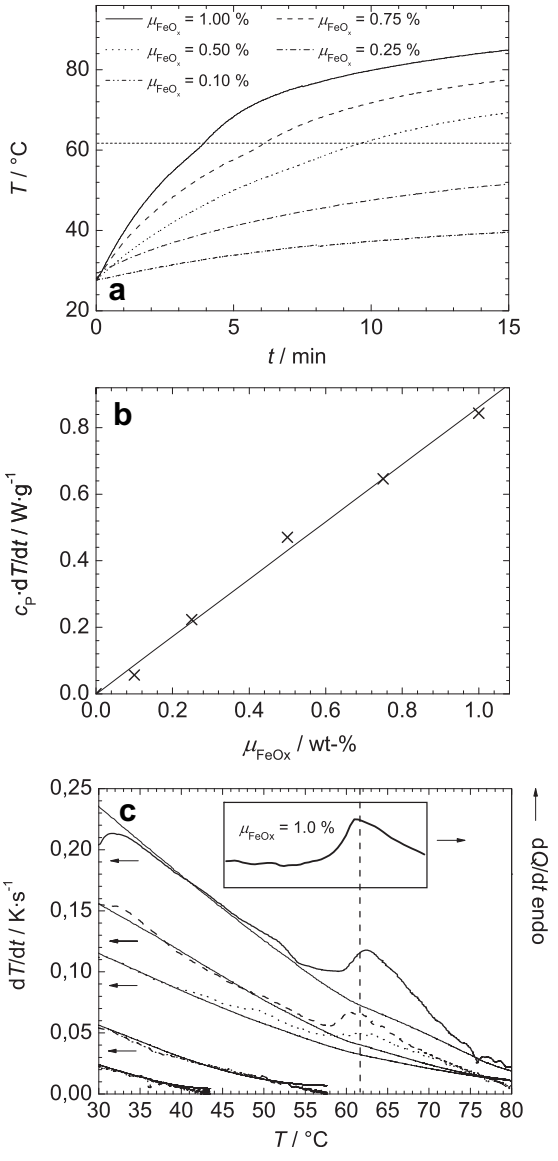

Fig. 5. (a) Sample temperature T vs. irradiation time t for FeO_x@P(OEGMA) nanoparticle dispersions in AC magnetic field (300 kHz, $H = 42.6$ kA m^{-1}); (b) heating power c_p(dT/dt)$_{t\to 0}$ from the thermograms vs. FeO_x content of FeO_x@P(OEGMA) nanoparticle dispersions in water; (c) differential magnetocalorimetric thermograms in comparison to logarithmic fits, and to a sample DSC thermogram (inset). compact line: $\mu_{FeOx} = 1.00$ mass-%; dashed line: $\mu_{FeOx} = 0.75$ mass-%; dotted line: $\mu_{FeOx} = 0.50$ mass-%; dash-dotted line: $\mu_{FeOx} = 0.25$ mass-%; dash-dot-dotted line $\mu_{FeOx} = 0.10$ mass-%.

experiments are performed in a vacuum-isolated glass sample container. Different samples with varying magnetite concentrations μ_{FeOx} of FeO_x@POEGMA nanoparticle based magnetic fluid in water were exposed to the oscillating magnetic field. Via a fiber-optical sensor the fluid temperature T was measured with time t. The resulting heating curves are presented in Fig. 5(a).

The temperature of all samples increases within minutes to temperatures up to 80 °C, depending on the FeO_x content. For each of the resulting thermograms, the early course of the graphs can be sufficiently described as resulting from a heat flux dQ/dt caused by the magnetic particles that is constant over time, and a logarithmic decrease of dT/dt with time due to heat loss to the environment. A higher FeO_x content leads to faster heating.

For each concentration, the heat flux dQ/dt per mass unit of fluid is calculated from the initial slope (dT/dt)$_{t\to 0}$

$$\frac{dQ}{dt} = \left(\frac{dT}{dt}\right)_{t\to 0} \times c_p \quad (1)$$

by estimating the specific heat capacity c_p from the composition of the fluid. A graph of dQ/dt over the magnetic mass fraction of the dispersion (by VSM) yields a linear relationship that is in accordance with the heating power as an intrinsic property of the cores for the given field parameters, and a specific heat power SHP = 86.5 W g^{-1} of the particle cores can be extracted from the slope.

$$\mathrm{SHP} = \frac{dQ}{dt} \times \frac{1}{\mu_{\mathrm{FeO}_x}} \quad (2)$$

The heat flux generated is strong enough to reach the cloud point temperature T_c of 61 °C in the dispersions at magnetic fractions of $\mu_{\mathrm{FeO}x} = 0.5$ mass-% and higher. In this temperature range, we observe a slight deviation from the expected logarithmic deceleration of the heating rate (Fig. 5a). We attribute the deviation to the heat consumption caused by the phase transition process. In order to confirm this, we compare the differential thermographs to logarithmic fits (Fig. 5c). The graphs of two samples with the highest particle content show a distinct deviation from the expected behavior in the temperature range of the LCST, that can be compared to the corresponding DSC thermogram and cloud point photometry of the same material. From DSC, we extract a demixing enthalpy of 5.99 kJ/mol with respect to the monomer units, in agreement with the contribution of one or more H bonds per monomer unit to the thermoreversible solvation process [41]. The value is in agreement with the micellization heat reported for one oxypropylene unit in triblock copolymers of poly(oxyethylene)-poly(oxypropylene)-poly(oxyethylene) [$(EO)_x(PO)_y$–$(EO)_x$] [42] that is mainly attributed to the dehydration of the hydrophobic ether group. The two processes can be suggested to be comparable in this respect, being confirmed by the enthalpic results.

The good correspondence of the peak observed in the magnetic thermograms with two independent methods indicates that the energy balance of the phase transition process is of enough impact to be observed in the magnetic heating experiments. Further optimization of this method will give more detailed insight into the processes involved.

4. Conclusion

Multifunctional hydrophilic nanostructures are reported that combine thermoflocculation and magnetic addressability in order to achieve particle dispersions that reversibly flocculate in AC magnetic fields.

The flocculation is due to the LCST behavior of the polymer shell in water, composed of a brush layer of oligo(ethylene glycol) methacrylate copolymers. We found that the phase transition temperature depends linearly on the copolymer composition. Therefore the phase transition is predictable and adjustable in a temperature range that is of interest for biomedical applications. Here, it may be of use that the phase separation facilitates the magnetic separation of the nano-objects with low magnetic field gradients.

Under the influence of an AC magnetic field, the aqueous particle dispersions show intrinsic heating, and the enthalpic process of phase transition can be monitored in the magnetic thermograms. By adjusting the transition temperature closer to body temperature, the effect may be used to manipulate particle behavior in biological systems.

Acknowledgement

We thank H. Ritter for his steady interest in our studies, and W. Frank and W. Kläui, Heinrich-Heine-Universität Düsseldorf (Germany) for TGA and NMR measurements. We gratefully acknowledge DFG for financial support within the Emmy-Noether program and the priority programs SPP 1104 and 1259.

References

[1] Bikram M, Gobin AM, Whitmire RE, West JL. J Controlled Release 2007;123(3):219–27.
[2] Pong FY, Lee M, Bell JR, Flynn NT. Langmuir 2006;22(8):3851–7.
[3] Wakamatsu H, Yamamoto K, Nakao A, Aoyagi T. J Magn Magn Mater 2006;302(2):327–33.
[4] Wang C, Flynn NT, Langer R. Adv Mater 2004;16(13):1074–9.
[5] Wang H, Peng M, Zheng J, Li P. J Colloid Interf Sci 2008;326(1):151–7.
[6] Sun Y, Ding X, Zheng Z, Cheng X, Hu X, Peng Y. Chem Commun 2006:2765–7.
[7] You Y-Z, Kalebaila KK, Brock SL, Oupicky D. Chem Mater 2008;20(10):3354–9.
[8] Edwards EW, Chanana M, Wang D. J Phys Chem C 2008;112(39):15207–19.
[9] Schmidt AM. Colloid Polym Sci 2007;285(9):953–66.
[10] Brazel C. Pharmaceut Res 2009;26(3):644–56.
[11] Gelbrich T, Feyen M, Schmidt AM. Macromolecules 2006;39(9):3469–72.
[12] Kaiser A, Gelbrich T, Schmidt AM. J Phys: Condens Matter 2006;18(38):S2563–80.
[13] Schmidt AM. Macromol Rapid Commun 2005;26(2):93–7.
[14] Ohnishi N, Furukawa H, Hideyuki H, Wang J-M, An C-I, Fukusaki E, et al. NanoBiotechnol 2006;2:43–9.
[15] Lai JJ, Hoffman JM, Ebara M, Hoffman AS, Estournes C, Wattiaux A, et al. Langmuir 2007;23(13):7385–91.
[16] Schild HG. Prog Polym Sci 1992;17(2):163–249.
[17] Heskins M, Guillet JE. J Macromol Sci A 1968;2(8):1441–55.
[18] Chanana M, Jahn S, Georgieva R, Lutz J-F, Bäumler H, Wang D. Chem Mater 2009;21(9):1906–14.
[19] Zhang MQ, Desai T, Ferrari M. Biomaterials 1998;19(10):953–60.
[20] Hu F, Neoh KG, Cen L, Kang E-T. Biomacromolecules 2006;7(3):809–16.
[21] Hergt R, Dutz S, Müller R, Zeisberger M. J Phys Condens Matter 2006;18(38):S2919–34.
[22] Müller G, Dutz S, Hergt R, Schmidt C, Steinmetz H, Zeisberger M, et al. J Magn Magn Mater 2007;310(2):2399–401.
[23] Glöckel G, Hergt R, Zeisberger M, Dutz S, Nagel S, Weitschies W. J Phys Condens Matter 2006;18(38):S2935–49.
[24] Gneveckow U, Jordan A, Scholz R, Bruss V, Waldofner N, Ricke J, et al. Med Phys 2004;31(6):1444–51.
[25] Falk MH, Issels RD. Int J Hyperthermia 2001;17(1):1–18.
[26] Fan QL, Neoh KG, Kang E-T, Shuter B, Wang S-C. Biomaterials 2007;28(36):5426–36.
[27] Lutz J-F, Stiller S, Hoth A, Kaufner L, Pison U, Cartier R. Biomacromolecules 2006;7(11):3132–8.
[28] Lutz J-F, Hoth A. Macromolecules 2006;39(2):893–6.
[29] Kamigaito M, Ando T, Sawamoto M. Chem Rev 2001;101(12):3689–745.
[30] Matyjaszewski K, Shipp DA, Wang J-L, Grimaud T, Patten TE. Macromolecules 1998;31(20):6836–40.
[31] Lutz J-F, Weichenhan K, Akdemir Ö, Hoth A. Macromolecules 2007;40(7):2503–8.
[32] Becer CR, Hahn S, Fijten MWM, Thijs HM, Hoogenboom R, Schubert US. J Polym Sci A Polym Chem 2008;46(21):7138–47.
[33] Kitano H, Hirabayashi T, Gemmei-Ide M, Kyogoku M. Macromol Chem Phys 2004;205(12):1651–9.
[34] Han S, Hagiwara M, Ishizone T. Macromolecules 2003;36(22):8312–9.
[35] Massart R, Cabuil VJ. Chem Phys 1987;84(7, 8):967–73.
[36] Biver C, Hariharan R, Mays J, Russel WB. Macromolecules 1997;30(6):1787–92.
[37] Chantrell R, Popplewell J, Charles S. IEEE Trans Magn 1978;14(5):975–7.
[38] Kaiser A, Winkler M, Krause S, Finkelmann H, Schmidt AM. J Chem Mater 2009;19(4):538–43.
[39] Neel L. Comptes Rendus Hebdomadaires Des Seances De L Academie Des Sciences 1949;228(1):64–6.
[40] Brown WF. J Appl Phys Suppl 1959;30:130.
[41] Saeki S, Kuwahara N, Nakata M, Kaneko M. Polymer 1976;17(8):685–9.
[42] Wanka G, Hoffmann H, Ulbricht W. Macromolecules 1994;27(15):4145–59.